Selective Early Cardiolipin Peroxidation after Traumatic Brain Injury: An Oxidative Lipidomics Analysis

Hülya Bayir, MD,[1–4] Vladimir A. Tyurin, PhD,[1,4] Yulia Y. Tyurina, PhD,[1,4] Rosa Viner, PhD,[5] Vladimir Ritov, PhD,[1] Andrew A. Amoscato, PhD,[6] Qing Zhao, MS,[1] Xiaojing J. Zhang, MS,[1] Keri L. Janesko-Feldman, BS,[2] Henry Alexander,[2] Liana V. Basova, PhD,[1,4] Robert S. B. Clark, MD,[2,3] Patrick M. Kochanek, MD,[2,3] and Valerian E. Kagan, PhD, DSci[1,4]

Objective: Enhanced lipid peroxidation is well established in traumatic brain injury. However, its molecular targets, identity of peroxidized phospholipid species, and their signaling role have not been deciphered.

Methods: Using controlled cortical impact as a model of traumatic brain injury, we employed a newly developed oxidative lipidomics approach to qualitatively and quantitatively characterize the lipid peroxidation response.

Results: Electrospray ionization and matrix-assisted laser desorption/ionization mass spectrometry analysis of rat cortical mitochondrial/synaptosomal fractions demonstrated the presence of highly oxidizable molecular species containing $C_{22:6}$ fatty acid residues in all major classes of phospholipids. However, the pattern of phospholipid oxidation at 3 hours after injury displayed a nonrandom character independent of abundance of oxidizable species and included only one mitochondria-specific phospholipid, cardiolipin (CL). This selective CL peroxidation was followed at 24 hours by peroxidation of other phospholipids, most prominently phosphatidylserine, but also phosphatidylcholine and phosphatidylethanolamine. CL oxidation preceded appearance of biomarkers of apoptosis (caspase-3 activation, terminal deoxynucleotidyltransferase–mediated dUTP nick end labeling–positivity) and oxidative stress (loss of glutathione and ascorbate).

Interpretation: The temporal sequence combined with the recently demonstrated role of CL hydroperoxides (CL-OOH) in in vitro models of apoptosis suggest that CL-OOH may be both a key in vivo trigger of apoptotic cell death and a therapeutic target in experimental traumatic brain injury.

Ann Neurol 2007;62:154–169

Polyunsaturated lipids have long been recognized as molecules indispensable for the structural and functional organization of the brain. Their roles as signaling molecules, as participants and coordinators of responses to physiological regulations, and as danger signals in injury, are not well known.[1,2] Because of their high susceptibility to attack by reactive oxygen species and oxidative modifications, peroxidation of polyunsaturated phospholipids is implicated in different types of brain damage. Yet, the specific functions and signaling roles of oxidized polyunsaturated phospholipids remain ill defined.[3] With the advent of mass spectrometry (MS)–based lipidomics, new perspectives in the identification of individual molecular species of phospholipids in brain functions have emerged.[4,5] However, MS analysis of *oxidized phospholipids* and their role in brain metabolic pathways, that is, oxidative lipidomics, is still poorly developed. This is mostly due to a large variety of low abundant species of peroxidized phospholipids combined with their relatively low stability during MS protocols.[6] With this in mind, we initiated oxidative lipidomics studies of brain injury. We were particularly interested in traumatic brain injury (TBI) using controlled cortical impact (CCI) model where spatial and temporal relationships between the initial damage and subsequent reactions and inflammatory/oxidative stress response are quite well-defined.[7,8]

TBI is an important contributor to the mortality and morbidity after trauma, which is the leading cause of death in infants and children.[9] TBI has been commonly associated with enhanced production of reactive oxygen species and reactive nitrogen species, antioxi-

From the [1]Center for Free Radical and Antioxidant Health, [2]Safar Center for Resuscitation Research, Departments of [3]Critical Care Medicine and [4]Environmental and Occupational Health, University of Pittsburgh, Pittsburgh, PA; [5]ThermoFisher Scientific, San Jose, CA; and [6]Department of Pathology, University of Pittsburgh, Pittsburgh, PA.

Received Mar 14, 2007, and in revised form May 14. Accepted for publication May 29, 2007.

Published online August 8, 2007 in Wiley InterScience (www.interscience.wiley.com). DOI: 10.1002/ana.21168

Address correspondence to Dr Bayir, 3434 Fifth Avenue, Pittsburgh, PA 15213. E-mail: bayihx@ccm.upmc.edu

dant depletion, and resulting oxidative stress.[10] We reported that TBI in children caused depletion of the major water-soluble antioxidant, ascorbate, and accumulation of S-nitrosylated thiols in cerebrospinal fluid.[11,12] Among different biomarkers of oxidative stress, enhanced lipid peroxidation is one of the most prominent.[13] Accumulation of end products of lipid peroxidation has been documented in brain and cerebrospinal fluid after experimental and clinical TBI in both adults and children, respectively.[7,11,14,15] However, essential information on molecular targets, particularly specific polyunsaturated molecular species of phospholipids undergoing oxidation, is lacking.

Assessment of isoprostanes and neuroprostanes has reliably established involvement of lipid peroxidation in central nervous system injury.[16] This approach, however, defines the fatty acid composition of modified substrates but leaves the origin and identity of oxidized phospholipids sepulchered. This deficiency makes it difficult to identify causal links among lipid peroxidation, oxidative phospholipid signaling, and mechanisms of cell injury and death. Attempts have been made to define individual phospholipid classes undergoing oxidation. Cardiolipin (CL), a mitochondria-specific phospholipid, has been suggested to be a preferred oxidation substrate in neuronal injury.[17–19] However, these assessments were mostly based on the use of nonspecific fluorescent techniques utilizing nonyl acridine orange as a CL-binding reagent. The validity of this protocol has been criticized.[20,21] It has been demonstrated that cells lacking CL-synthase, completely devoid of CL, displayed a similar pattern of nonyl acridine orange responses as wild-type cells.[22] Moreover, the fluorescence response of the probe is obscured by its membrane potential–driven partition into different mitochondrial compartments and the respiration state.[20]

We recently developed an oxidative lipidomics approach that includes quantitative assessments of hydroperoxides in different major classes of phospholipids combined with their MS characterization. We discovered that oxidation of a CL catalyzed by cytochrome *c* was an early characteristic of mitochondrial response to proapoptotic challenges in vitro.[23] Accumulation of CL oxidation products was essential for the release of proapoptotic factors, including cytochrome *c*. The role of CL oxidation in the execution of the apoptotic program in vivo has not been addressed.

In this study, we applied oxidative lipidomics to analyze phospholipid oxidative modifications after TBI in vivo. We used our established CCI model in 17-day-old rats[24] in which the formation of functioning synapses in neuronal development is analogous to developmental processes in the young child.[25] By comparing oxidized molecular species and classes of phospholipids with their abundance, we identified the species of phospholipids most susceptible to peroxidation. We established that CL, predominantly its molecular species containing $C_{22:6}$, is a specific, early, and prominent target for TBI-induced oxidative injury. This suggests that CL oxidation products may signal apoptotic cell death in brain in vivo, and thus represent both a putative early biomarker of apoptosis and a key acute therapeutic target.

Materials and Methods

Controlled Cortical Impact Model

Seventeen-day-old male Sprague–Dawley rats were anesthetized with 3.5% isoflurane in O_2. The trachea was intubated with a 14-gauge angiocatheter. Anesthesia was maintained with 2% isoflurane in N_2O/O_2 (2:1). A rectal probe was inserted for temperature monitoring. The head was fixed in a stereotactic device. A craniotomy was made over the left parietal cortex with a dental drill, using the coronal and interparietal sutures as margins. A microprobe (Physitemp Instruments, Clifton, NJ) was inserted through a burr hole into the left frontal cortex to monitor brain temperature. Rats were warmed using a heat lamp to a brain temperature of 37 ± 0.5°C, isoflurane was decreased to 1%, and they were then allowed to equilibrate (30 minutes). For all studies, a 6mm metal pneumatically driven impactor tip was used; velocity was 4.0 ± 0.2m/sec, depth of penetration was 2.5mm, and duration of deformation was 50 milliseconds. After TBI, the bone flap was replaced, sealed with dental cement, and the scalp incision was closed. After a 1-hour monitoring period, rats were weaned from mechanical ventilation, extubated, and returned to their cages until further study. A mortality rate of $\leq$5% is routinely observed with this protocol by our group.[24]

ISOLATION OF CRUDE MITOCHONDRIAL/SYNAPTOSOMAL (P2) FRACTION. The crude brain mitochondrial fraction was prepared as described previously.[26] In brief, rats were perfused transcardially with ice-cold saline and then decapitated, brains (minus cerebellum) were rapidly removed, and ipsilateral pericontusional cortex was isolated and placed in 10 volumes of ice-cold 0.32M sucrose in 10mM tris(hydroxymethyl)aminomethane buffer (pH 7.4). The tissue was homogenized in a Teflon/glass homogenizer (clearance, 0.1–0.15mm) by 10 gentle up-and-down strokes. The homogenate was spun at 1,000*g* for 10 minutes to remove nuclei and cell debris. The resulting supernatant was centrifuged at 10,000*g* for 20 minutes to obtain the crude mitochondrial pellet. The final pellet was washed and centrifuged (4 minutes, 10,000*g*, 4°C). It has been shown that this protocol yields P2 fraction with relatively high content of synaptosomal mitochondria.[27] In addition, P2 fraction contains nonsynaptosomal mitochondria, synaptosomal membranes, and plasma membranes,[28] as evidenced by relatively high content of phosphatidylserine (PS; see later). We chose to use crude mitochondrial/synaptosomal fraction in the study to prevent selective isolation of only undamaged mitochondria from CCI samples.

LIPID EXTRACTION AND TWO-DIMENSIONAL HIGH-PERFORMANCE THIN-LAYER CHROMATOGRAPHY ANALYSIS. Total lipids were extracted from mitochondria using the Folch procedure.[29] Lipid extracts were separated and analyzed by two-dimensional high-performance thin-layer chromatography (2D-HPTLC) on silica G plates (5 × 5cm; Whatman, Florham Park, NJ).[30] The plates were first developed with a solvent system consisting of chloroform/methanol/28% ammonium hydroxide (65:25:5 vol/vol). After the plate was dried with a forced N2 blower to remove the solvent, it was developed in the second dimension with a solvent system consisting of chloroform/acetone/methanol/glacial acetic acid/water (50:20:10:10:5 vol/vol). The phospholipids were visualized by exposure to iodine vapors and identified by comparison with authentic phospholipid standards. Lipid phosphorus was determined by a micromethod.[31]

Phospholipid hydroperoxides were determined by fluorescence high-performance liquid chromatography (HPLC) of products formed in microperoxidase-11–catalyzed reaction with Amplex Red, *N*-acetyl-3,7-dihydroxyphenoxazine (Molecular Probes, Eugene, OR) as described previously.[23] Oxidized phospholipids were hydrolyzed by porcine pancreatic phospholipase A_2 (2U/μl) in 25mM phosphate buffer containing 1.0mM Ca, 0.5mM EDTA, and 0.5mM sodium dodecyl sulfate (pH 8.0 at room temperature for 30 minutes). After that 50μM Amplex Red and microperoxidase-11 (1.0μg/μl) was added and samples were incubated at 4°C for 40 min. The reaction was terminated by addition of 100μl stop reagent (10mM HCl, 4mM butylated hydroxytoluene [BHT] in ethanol). After centrifugation at 15,000*g* for 5 minutes, aliquots of supernatant (5μl) were injected into Eclipse XDB-C18 column (5μm, 150 × 4.6mm). The mobile phase was composed of 25mM NaH_2PO_4 (pH 7.0)/methanol (60:40 vol/vol). The flow rate was 1ml/min. Resorufin (an Amplex Red oxidation product) fluorescence (λ_{ex} 560nm, λ_{em} 590nm) was measured by Shimadzu LC-100AT vp HPLC system equipped with fluorescence detector (RF-10Axl) (Shimadzu, Kyoto, Japan) and autosampler (SIL-10AD vp). Data were processed and stored in digital form with Class-VP software.

Mass spectra of phospholipids were analyzed by direct infusion into a triple-quadrupole mass spectrometer (Finnigan MAT TSQ 700; ThermoFisher Scientific, San Jose, CA), a Quattro II triple quadrupole mass spectrometer (Micromass, Manchester, United Kingdom), or a quadrupole linear ion trap mass spectrometer (LXQ; ThermoFisher Scientific). After 2D-HPTLC separation samples were collected, evaporated under N_2, resuspended in chloroform/methanol 1:2 vol/vol (20pmol/μl), and used for acquisition of negative ion electrospray ionization (ESI) mass spectra at a flow rate of 5μl/min. The electrospray probe was operated at a voltage differential of −3.5 to 5.0kV in the negative or positive ion mode. Source temperature was maintained at 70°C in the case of triple-quadrupole mass spectrometers and 150°C for capillary temperature of ion trap LXQ. In addition, MS analysis was performed on a Finnigan LTQ mass spectrometer with MALDI source (ThermoFisher Scientific). Lipid samples were dissolved in chloroform/methanol 1:1 vol/vol. One microliter of lipid solution was spotted directly onto a MALDI plate and dried. A total of 0.5μl of 2,5-dihydroxybenzoic acid (25mg/ml in chloroform/methanol 1:1 vol/vol) was added to each spot as matrix. Spectra were acquired in negative ion mode using full-range zoom (m/z 500–2,000) or ultrazoom (SIM) scans. Tandem mass spectrometry (MS/MS) analysis of individual phospholipid species was used to determine the fatty acid composition. Collision-induced dissociation spectra on triple-quadrupole instruments were obtained by selecting the ion of interest and performing daughter ion scanning in Q3 at 400Da/sec using Ar as the collision gas. MS^n analysis on ion trap instruments was conducted with relative collision energy ranged from 20 to 40%, and with activation *q* value at 0.25 for collision-induced dissociation and 0.7 for pulsed-Q dissociation technique.

Clusters of signals with a mass difference of 16 known to represent two forms of glycerophospholipids, alkenyl-acyl and diacyl species, were detectable in ESI-MS spectra.[32] MS/MS fragmentation of ether-linked alkenyl (plasmalogen) species resulted in the formation of two typical product ions formed after loss of fatty acyl in sn-2 position: mono-lyso-alkenyl species and mono-lyso-acyl species. To further confirm the identity of glycerophospholipids, we exposed them to HCl fumes known to hydrolyze alkenyl-acyl glycerophospholipids to yield their lyso-acyl derivatives. The reaction products were subjected to HPTLC, and spots corresponding to glycerophospholipids were analyzed by ESI-MS. This treatment resulted in disappearance of molecular ions corresponding to molecular species of alkenyl-acyl glycerophospholipids, whereas those of diacyl phospholipids remained unchanged. MS/MS fragmentation of ether-linked alkyl-acyl-glycerophospholipids in negative mode yielded two typical deprotonated product ions formed after the loss of fatty acyl in sn-2 position: mono-lyso-alkyl species and acyl species. Product ions representing mono-lyso-alkyl species have mass differences of 14 compared with the product ions of corresponding mono-lyso-acyl species. Finally, chemical structures of glycerophospholipids were confirmed by Lipid Map Data Base using ChemDraw format (www.lipidmaps.org).

Histological Assessment

Neurodegeneration in the pericontusional area was assessed using terminal deoxynucleotidyltransferase–mediated dUTP nick end labeling (TUNEL) on 5μm paraffin sections cut through the dorsal hippocampus as described previously.[33]

Caspase-3 activity was measured using Caspase-Glo assay kit obtained from Promega (Madison, WI). Caspase-3 activity was expressed as the luminescence produced within 1 hour of incubation at 25°C using a ML1000 luminescence plate reader (Dynatech Labs, Chantilly, VA).

FLUORESCENCE ASSAY OF REDUCED GLUTATHIONE. Glutathione (GSH) levels were estimated in cortical homogenates using ThioGloTM-1[34] as described previously with minimal modifications.[7] GSH concentrations were determined by addition of GSH peroxidase and hydrogen peroxide to the brain homogenates, and the resultant fluorescence response was subtracted from the fluorescence response of the same specimens without addition of GSH peroxidase and hydrogen peroxide (Sigma, St. Louis, MO). A Shimadzu spectrophotometer RF-5301PC (Shimadzu, Kyoto, Japan)

was employed using 388nm (excitation) and 500nm (emission) wavelengths.

HIGH-PERFORMANCE LIQUID CHROMATOGRAPHY ASSAY OF ASCORBATE. Supernatant obtained after precipitation of proteins in brain homogenates by 10% trichloroacetic acid and sedimentation (2,000*g* × 10 minutes) was used for HPLC measurements, as described previously.[7]

Mitochondrial electron transport was determined by measuring the rotenone-sensitive NADH oxidase activity in an HPLC-based assay as described previously.[35,36] To provide access of NADH to synaptic mitochondria, we treated the aliquots of mitochondria fractions by nitrogen cavitation.[37] In these experiments, CL content in mitochondria samples was measured using an HPLC-based assay, as described previously.[38]

Statistical Analysis

Data are expressed as mean ± standard deviation. Brain oxidized phospholipid, GSH and ascorbate levels, and caspase-3/7 activity were compared among different groups using analysis of variance with Tukey's posttest. Rotenone-sensitive NADH:O_2 oxidoreductase activity between sham and CCI was compared using *t* test. Histological sections were assessed semiquantitatively by one of the authors masked to the study groups.

Results

Phospholipid Composition

Mitochondria, particularly synaptic mitochondria, are believed to play a pivotal role in oxidative brain injury.[39–41] Therefore, we used a mitochondria-rich synaptosomal fraction (P2) isolated from postnatal day 17 rats for our studies.

Figure 1 shows a typical 2D-HPTLC profile of major classes of phospholipids in the isolated P2 fractions. The silica spots were scraped off the plate, and the phospholipid content was quantified via the amounts of phosphatidylinositol (Table 1). TBI did not induce any significant change in the phospholipid composition of P2 fractions compared with controls except for the accumulation of lysophosphatidylcholine. This is consistent with the scale of accumulation of oxidation products not exceeding 5mol% of individual phospholipids (see later).

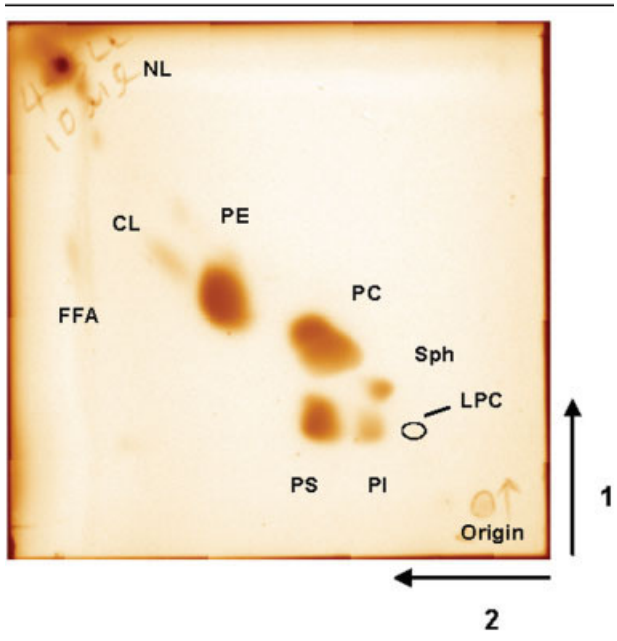

Fig 1. Typical two-dimensional high-performance thin-layer chromatography of total lipids extracted from cortical P2 fraction. CL = cardiolipin; FFA = free fatty acids; LPC = lysophosphatidylcholine; NL = neutral lipids; PC = phosphatidylcholine; PE = phosphatidylethanolamine; PI = phosphatidylinositol; PS = phosphatidylserine; Sph = sphingomyelin.

Table 1. **Phospholipid Composition of P2 Fraction Isolated from Ipsilateral (Left) Cerebral Cortex (% of Total)**

Phospholipid Class	Control	Trauma
Cardiolipin	2.4 ± 0.3	1.9 ± 1.2
Phosphatidylethanolamine	37.7 ± 1.0	36.1 ± 0.7
Phosphatidylcholine	43.0 ± 1.8	43.3 ± 0.7
Phosphatidylserine	12.4 ± 0.7	12.3 ± 0.1
Phosphatidylinositol	3.4 ± 0.3	3.3 ± 0.4
Sphingomyelin	1.3 ± 0.7	1.6 ± 1.0
Lysophosphatidylcholine	<0.5	1.4 ± 0.8

Mass Spectroscopic Analysis of Individual Molecular Species

We further used ESI- and MALDI-MS to characterize individual molecular species of phospholipids in P2 fractions. We present detailed description of MS experiments with CL because identification of its molecular species is technically more challenging than of other phospholipids.

CL possesses two anionic charges that form both singly charged $[M-H]^-$ and doubly charged $[M-2H]^{-2}$ ions (Fig 2Aa). The identities of major CL clusters and their structures were analyzed by tandem MS using the approach that Hsu and Turk[42] described. Molecular species of brain CL were represented by at least 12 different major clusters with a variety of fatty acid residues. These included polyunsaturated arachidonic ($C_{20:4}$) and docosahexaenoic ($C_{22:6}$) (DHA) fatty acids highly susceptible to peroxidation. As an example, Figure 2Ab shows a typical MS/MS fragmentation experiment. The major CL molecular cluster of singly charged CL ion at m/z 1,550.2, which corresponds to doubly charged CL ion at m/z 774.5, yielded ions with

m/z 279, 281, 283, 303, 305, 327, and 329. These signals correspond to $C_{18:2}$, $C_{18:1}$, $C_{18:0}$, $C_{20:4}$, $C_{20:3}$, $C_{22:6}$, and $C_{22:5}$ fatty acids, which originate from at least four different CL molecular species as follows: $(C_{18:1})_1/(C_{18:0})_1/(C_{22:6})_2$; $(C_{18:0})_1/(C_{20:4})_2/(C_{22:5})_1$; $(C_{18:2})_1/(C_{20:3})_2/(C_{22:5})_1$; and $(C_{18:2})_1/(C_{18:0})_1/(C_{22:5})_1/(C_{22:6})_1$. Complete structural characterization of major CL clusters by multistage fragmentation (MS^n) using ion trap MS identified at least two isomers in each of the CL molecular species as summarized in Table 2.

These characterizations were confirmed by MALDI-MS^n. Typical ions formed during fragmentation process of CL (*a, b, a*+136, or *b*+136) were identified in MS^2 spectra.[42] Then MS^3 was performed on each of *a* or *b* ions to assign fatty acids and their positions. As an example, Figure 2Bb shows analysis of one of the precursors detected at m/z 1,472. During MALDI ionization, both $[M-H]^-$ and $[M-2H+Na]^-$ types of ions and ions of adducts with DHB matrix are formed. Three types of ions ($[M-H]^-$, $[M-2H+Na]^-$, $[M-2H+DHB+Na]^-$) and seven predominant molecular species, including four isomers, (of the *a/b* or (*a*+136)/(*b*+136) ion pairs) were identified from analysis of just one precursor in the MS^2 spectrum of the m/z 1,472 ion (see Fig 2B,b). The most dominant ion $[M-2H+Na]^-$ consisted of at least four isomers that were identified as $(C_{16:1}/C_{18:1})(C_{18:2}/C_{20:3})$; $(C_{18:2}/C_{20:4})(C_{16:0}/C_{18:1})$; $(C_{18:2}/C_{18:1})(C_{16:1}/C_{20:4})$; and $(C_{18:1}/C_{18:2})(C_{18:2}/C_{18:2})$. These isomers of CL, corresponded to doubly charged ion at m/z 724.2 (see Fig 2A). The ion $[M-H]^-$ consisted of $(C_{18:1}/C_{18:1})(C_{16:2}/C_{22:6})$ and $(C_{16:1}/C_{20:4})(C_{18:2}/C_{20:3})$. Matrix adduct ion $[M-2H+DHB+Na]^-$ corresponded to $(C_{14:0}/C_{14:0})/(C_{16:0}/C_{16:0})$.

In contrast with multiple species of CL, a single major molecular ion of PS with m/z 834 was observed using negative ionization mode (Fig 3A). PS fragmentation yielded a strong peak with m/z 747 caused by loss of the serine group. Molecular fragments with m/z 283 and 327 correspond to carboxylate anions of stearic acid ($C_{18:0}$) and DHA ($C_{22:6}$), respectively.

We used ESI-MS analysis to characterize individual molecular species of phosphatidylinositol, phosphatidylethanolamine (PE), phosphatidylcholine (PC), and sphingomyelin as well. The distribution of molecular species in these phospholipids, as well as characteristic fragments obtained by their fragmentation, are summarized in Table 3. Note that all major phospholipids (CL, PS, PE, and PC) contained molecular species with polyunsaturated fatty acid residues, particularly $C_{20:4}$, $C_{22:5}$, and $C_{22:6}$. These polyunsaturated fatty acids are known to be most susceptible to oxidative attack. Thus, random oxidation should cause oxidation of all of these phospholipid classes.

Phospholipid Oxidation and Identification of Individual Oxidized Molecular Species

Next, we used ESI-MS to detect and identify molecular species of phospholipids that underwent oxidation at 3 and 24 hours after CCI. Comparison of the CL spectra from ipsilateral cortex in control and CCI rats demonstrated an increased intensity of a peak at m/z 790.6. Detailed analysis of this peak demonstrated that the $[M-2H]^{2-}$ ion corresponds to multiple CL species with a dominant isomer of $(C_{18:1}/C_{22:6})(C_{22:6+OOH}/C_{18:0})$ originating from the ion at m/z 774.8 (see Fig 2C). The structural assignment of this CL-OOH product with hydroperoxy group in $C_{22:6}$ was obtained by MS^n fragmentation as described earlier (data not shown). MALDI-MS analysis confirmed this conclusion (data not shown). We performed oxidative lipidomics analysis of doubly charged species for CL because the signal intensity of doubly charged ion is higher compared with the singly charged one as shown in Figure 2A.

MS analysis of PS in the ipsilateral cortex in control and CCI rats detected presence of PS molecular species with oxidized $C_{22:6}$, PS-OOH, with m/z 866 (see Fig 3B). The intensity of this signal was higher at 24 hours

Fig 2. Typical negative ion electrospray ionization (ESI) (A) and matrix-assisted laser desorption/ionization (MALDI) (B) mass spectra of cardiolipins (CLs) obtained from cortical P2 fraction. CLs isolated by two-dimensional high-performance thin-layer chromatography (2D-HPTLC) were subjected to mass spectrometry (MS) analysis by direct infusion into mass spectrometer. (A) The identities of major molecular species in CL clusters were established by tandem MS. Shown is a typical MS/MS fragmentation experiment for a major CL molecular cluster with a single charged ion at m/z 1,550. Note the formation of ions with m/z 279, 281, 283, 303, 305, 327, and 329 corresponding to $C_{18:2}$, $C_{18:1}$, $C_{18:0}$, $C_{20:4}$, $C_{20:3}$, $C_{22:6}$, and $C_{22:5}$ fatty acids and resulting in at least four different CL molecular species as follows: $(C_{18:1})_2/(C_{18:0})_1/(C_{22:6})_2$; $(C_{18:0})_1/(C_{20:4})_2/(C_{22:5})_1$; $(C_{18:2})_1/(C_{20:3})_2/(C_{22:5})_1$; $(C_{18:2})_1/(C_{18:0})_1/(C_{22:5})_1/(C_{22:6})_1$ fatty acids (A, b). (B) Structural characterization of CL molecular species consisting of multiple isomers by Ion Trap MS^n fragmentation (B, b). MS^2 spectrum shows a singly charged CL ion at m/z 1,472; note the presence of multiple a and b fragments. (B, c) MS^3 spectrum of (a+136) *ion at m/z 829 of one of the 72:7 CL isomers. The MALDI-MS^3 spectrum of m/z 829 (1,472–829) ion confirmed the structure as $(C_{16:1})/(C_{18:1})$. All ion assignments were performed according to Hsu and Turk.[42] (C) Typical negative ion ESI mass spectra of molecular species of CL isolated from ipsilateral cortical P2 fraction after CCI. Identification of individual oxidized molecular species ($C_{22:6}$ containing CL-OOH). Tandem MS/MS experiments confirmed the structures of oxidized CL (C, a and b).*

after CCI versus control. Detailed analysis of this peak by ESI-MS demonstrated that the $[M-H]^-$ ion at m/z 866.4 corresponds to PS with dominating product of ($C_{18:0}/C_{22:6+OOH}$) originating from the ion at m/z 834 ($C_{18:0}/C_{22:6}$).

Consistent with the MS measurements, quantitative analysis of phospholipid oxidation by HPLC showed that CL underwent most robust and early (at 3 hours) oxidation after CCI (Fig 4). At this time point, no other phospholipids were oxidized. At 24 hours after

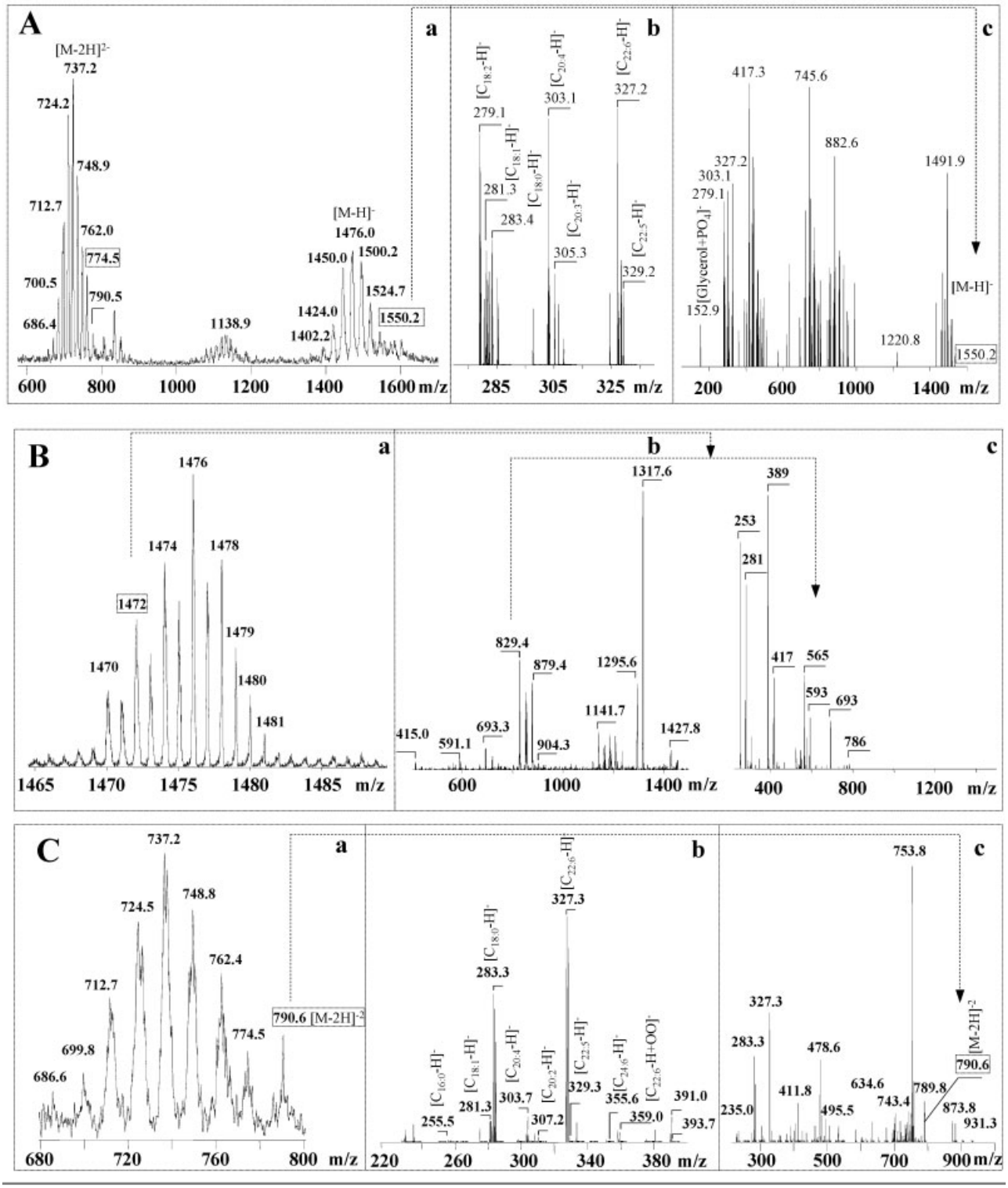

Figure 2

Table 2. **Major Cardiolipin Molecular Species from P2 Fraction of Rat Brain Cortex**

Molecular Species	m/z $[M-2H]^{-2}$	m/z $[M-H]^{-}$	Acyl Chain Composition
Cardiolipin			
Diacyl species of major clusters			*Acyl/Acyl*
68:3	686.6	1,374.2	$(C_{14:0})_1/(C_{16:1})_1/(C_{18:1})_2$
68:3	700.5	1,402.0	$(C_{16:1})_1/(C_{16:0})_1/(C_{18:1})_2$
68:2	701.9	1,404.8	$(C_{16:0})_2/(C_{18:1})_2$
70:6	711.8	1,424.6	$(C_{16:0})_1/(C_{16:1})_1/(C_{18:1})_1/(C_{20:4})_1$
70:5	712.7	1,426.4	$(C_{16:1})_1/(C_{18:2})_1/(C_{18:1})_2$
70:4	713.9	1,428.8	$(C_{16:1})_1/(C_{18:1})_3$
72:8	723.5	1,448.0	$(C_{16:1})_1/(C_{18:2})_1/(C_{18:1})_1/(C_{20:4})_1$
72:8	723.5	1,448.0	$(C_{18:2})_4$
72:7	724.5	1,450.0	$(C_{16:1})_1/(C_{18:2})_1/(C_{18:1})_1/(C_{20:3})_1$
74:8	737.2	1,476.4	$(C_{18:1})_2/(C_{18:2})_1/(C_{20:4})_1$
76:11	748.8	1,498.6	$(C_{18:2})_1/(C_{18:1})_1/(C_{20:4})_2$
76:10	749.8	1,500.2	$(C_{18:1})_2/(C_{20:4})_2$
76:9	750.8	1,502.6	$(C_{16:0})_1/(C_{18:1})_1/(C_{20:4})_1/(C_{22:4})_1$
78:15	758.9	1,518.9	$(C_{16:1})_1/(C_{18:2})_1/(C_{22:6})_2$
78:14	759.5	1,520.0	$(C_{18:2})_1/(C_{20:4})_3$
78:12	762.0	1,524.0	$(C_{18:1})_2/(C_{20:4})_1/(C_{22:6})_1$
78:10	763.8	1,528.6	$(C_{18:1})_2/(C_{20:4})_1/(C_{22:4})_1$
80:13	774.5	1,550.0	$(C_{18:1})_1/(C_{18:0})_1/(C_{22:6})_2$
80:13	774.5	1,550.0	$(C_{18:0})_1/(C_{20:4})_2/(C_{22:5})_1$
80:13	774.5	1,550.0	$(C_{18:2})_1/(C_{20:3})_2/(C_{22:5})_1$
80:13	774.5	1,550.0	$(C_{18:2})_1/(C_{18:0})_1/(C_{22:5})_1/(C_{22:6})_1$
80:12	776.0	1,553.0	$(C_{18:0})_2/(C_{22:6})_2$
82:17	784.6	1,570.2	$(C_{18:1})_1/(C_{20:4})_1/(C_{22:6})_2$
82:11	790.6	1,582.7	$(C_{18:1})_1/(C_{20:2})_2/(C_{24:6})_1$

Phospholipids are designated as follows: tetra-acyl 74:8 cardiolipin (CL), where 74 indicates the summed number of carbon atoms at both the sn-1, sn-2, and sn-1′, sn-2′ positions and :8 designates the summed number of double bonds at both the sn-1, sn-2, and sn-1′, sn-2′ positions. Possible major species are indicated as tetra-acyl $(C_{18:1})_2/(C_{18:2})_1/(C_{20:4})_1$, where 18, 18, 18, and 20 are the numbers of carbon atoms in fatty acyl chains at the sn-1, sn-2 and sn-1′, sn-2′ positions, respectively, and :1, :1, :2, and :4 are the numbers of double bonds of the sn-1, sn-2 and sn-1′, sn-2′ fatty acyl chains, respectively. These individual CL molecular species were detected by ESI as deprotonated species of CL in the negative ionization mode at m/z ratios of 737.2 and 1,476.4. These m/z values indicate ratios of mass to charge for singly charged $[M-H]^{-}$ ions and doubly charged $[M-2H]^{-2}$ ions, respectively.

TBI, a marked oxidation of PS occurred, whereas other phospholipids such as PE and PC were only slightly oxidized. Importantly, the pattern of phospholipid oxidation was nonrandom and did not follow their abundance in P2 fraction (compare with Table 1).

Cytochrome c*–Catalyzed Oxidation of Tetralinoleyl-Cardiolipin*

To investigate interaction between cytochrome *c* and CL, we performed in vitro assessments of the ability of cytochrome *c* to catalyze H_2O_2-dependent peroxidation of polyunsaturated tetralinoleyl-cardiolipin. Marked accumulation CL hydroperoxides (CL-OOH) formed in this system was detected using fluorescence HPLC protocol (Fig 5A). We then identified the major oxidation products by ESI-MS. We found that molecular species of CL containing 1, 2, 3, 4, and 5 hydroperoxy groups were generated in the course of cytochrome *c*–catalyzed reaction (see Fig 5B). In addition, several hydroxy and hydroxy-hydroperoxy derivatives of CL were detected by MS analysis. This demonstrates that nonoxidized CL undergoes oxidation to its hydroperoxides in the presence of H_2O_2. Moreover, these results also show that cytochrome *c* can uti-

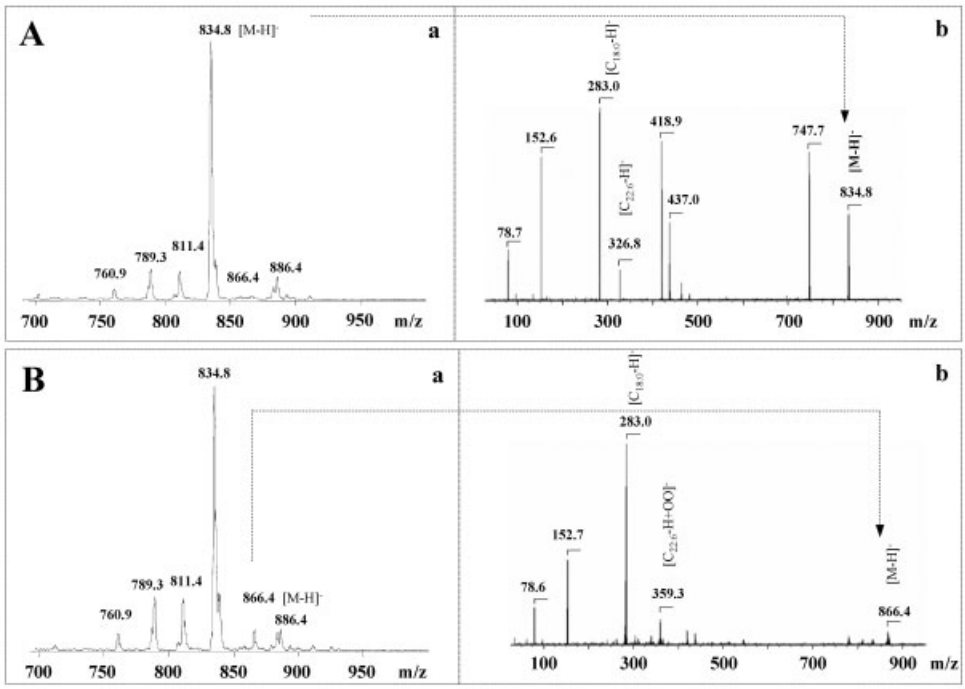

Fig 3. Typical negative ion ESI mass spectra of molecular species of phosphatidylserine (PS). Phospholipids isolated by two-dimensional high-performance thin-layer chromatography (2D-HPTLC) were subjected to mass spectrometry (MS) analysis by direct infusion into mass spectrometer. (A) Shown is a typical MS/MS fragmentation experiment for the major PS with m/z 834. PS fragmentation yielded a strong peak with m/z 747 caused by loss of the serine group. Molecular fragments with m/z 283 and 327 corresponded to carboxylate anions of stearic ($C_{18:0}$) and docosahexaenoic ($C_{22:6}$) fatty acids, respectively. (B) Typical negative ion ESI mass spectra of PS isolated from ipsilateral cortical P2 fraction after CCI. Identification of individual oxidized molecular species ($C_{22:6}$ containing PS-OOH). Tandem MS/MS experiments confirmed the structures of oxidized PS (B, a and b).

lize CL-hydroperoxides as a source of oxidizing equivalents to oxidize CL and simultaneously reduce CL-OOH to CL-OH.

Biomarkers of Cell Degeneration and Apoptosis

To determine whether there was a correspondence between phospholipid oxidation and the appearance of biomarkers of cell damage, we assessed time course of biomarkers of apoptosis. TUNEL-positivity was observed in the pericontusion cortical area at 24 hours after injury. There was no TUNEL-positive staining in sham-operated rat cortex (Fig 6A). Ipsilateral cortical caspase-3/7 activity was increased at 24 hours after CCI but not at 3 hours compared with control (see Fig 6B).

Assessments of Oxidative Stress and Mitochondrial Electron Transport Activity

GSH and ascorbate are two major water-soluble antioxidants in the brain.[43] Ipsilateral cortical GSH levels were decreased at 24 hours (10.84 $\pm$ 0.64nmol/mg protein) after CCI versus controls (14.56 $\pm$ 1.16nmol/mg protein) (Fig 7A). Ascorbate concentrations in ipsilateral cortex were lower at 24 hours in injured rats (43.02 $\pm$ 1.13nmol/mg protein) versus control rats (58.0 $\pm$ 4.74nmol/mg protein; $p < 0.05$) (see Fig 7B). Furthermore, the reductions in GSH and ascorbate levels correlated temporally with the nonspecific oxidation of phospholipids.

CL is essential for the maintenance of mitochondrial electron transport. We reasoned that CL oxidation could be associated with the loss of electron transport activity. In accord with this, we observed a significant decrease in rotenone-sensitive NADH:O_2 oxidoreductase activity at 3 hours after CCI versus control, coincident with the CL oxidation (see Fig 7C). There was no difference in cytochrome *c* oxidase subunit IV expression assessed by Western blot analysis between CCI and control (data not shown).

Discussion

Selective Early Oxidation of Cardiolipin: A Specific Apoptotic Trigger in Injured Brain?

This report presents the first detailed MS-based characterization of individual molecular species of major phospholipids in the rat cortex. Our emphasis has been placed on polyunsaturated molecular species of mitochondrial/synaptosomal phospholipids, particularly on the species containing DHA residues, as most likely targets for oxidative attack. We found that essentially

Table 3. **Major Phospholipid Molecular Species from P2 Fraction of Rat Brain Cortex**

Molecular Species	m/z $[M-H]^-$	Identified Acyl Chains
Phosphatidylinositol		
Diacyl species		*Acyl/Acyl*
34:1	835.8	$C_{16:1}/C_{18:0}$
36:4	857.8	$C_{16:0}/C_{20:4}$
38:4	885.8	$C_{18:0}/C_{20:4}$
38:3	887.8	$C_{18:0}/C_{20:3}$
40:6	909.8	$C_{18:0}/C_{22:6}$
Phosphatidylserine		
Diacyl species		*Acyl/Acyl*
34:1	760.8	$C_{16:0}/C_{18:1}$
36:1	788.8	$C_{18:0}/C_{18:1}$
38:4	810.8	$C_{18:0}/C_{20:4}$ and $C_{16:0}/C_{22:4}$
40:6	834.8	$C_{18:0}/C_{22:6}$
40:5	836.8	$C_{18:0}/C_{22:5}$
40:4	838.8	$C_{18:0}/C_{22:4}$
Phosphatidylethanolamine		
Diacyl species		*Acyl/Acyl*
38:6	762.8	$C_{16:0}/C_{22:6}$
38:4	766.8	$C_{18:0}/C_{20:4}$ or $C_{16:0}/C_{22:4}$
40:6	790.8	$C_{18:0}/C_{22:6}$
40:4	794.7	$C_{18:0}/C_{22:4}$
Alkenyl-acyl species		*Ether/Acyl*
34:1	700.8	$C_{16:0p}/C_{18:1}$
36:4	722.8	$C_{16:0p}/C_{20:4}$
38:5 or 38:6	747.8	$C_{18:1p}/C_{20:4}$ or $C_{16:0p}/C_{22:6}$
38:4	750.8	$C_{16:0p}/C_{22:4}$ or $C_{18:0p}/C_{20:4}$
38:2	754.7	$C_{18:0p}/C_{20:2}$ or $C_{18:1p}/C_{20:1}$
40:6	774.7	$C_{18:0p}/C_{22:6}$
40:4	778.8	$C_{18:0p}/C_{22:4}$
Sphingomyelin (sodium salt of molecular ion of m/z 731.7)		
Sphingoid base-acyl species		Sphingoid base/acyl
34:1	703.7	$C_{18:1}/C_{16:0}$
36:2	729.7	$C_{18:1}/C_{18:1}$
36:1	731.7	$C_{18:1}/C_{18:0}$
36:1	753.8*	$C_{18:1}/C_{18:0}$
38:1	759.8	$C_{18:1}/C_{20:0}$
42:2	813.8	$C_{18:1}/C_{24:1}$

all phospholipid classes (PC, PE, phosphatidylinositol, and CL) included $C_{22:6}$-containing species. This suggests that during a random nonenzymatic process of lipid peroxidation, phospholipids should be involved in the reaction proportionally to their abundance. Here we report that CCI-induced lipid peroxidation did not

Table 3. **continued**

Molecular Species	m/z $[M+H]^+$	Identified Acyl Chains
Phosphatidylcholine		
Diacyl species		*Acyl/Acyl*
30:0	706.7	$C_{14:0}/C_{16:0}$
32:1	732.7	$C_{16:0}/C_{16:1}$
32:0	734.7	$C_{16:0}/C_{16:0}$
34:2	758.8	$C_{16:1}/C_{18:1}$
34:1	760.7	$C_{16:0}/C_{18:1}$
34:0	762.7	$C_{16:0}/C_{18:0}$
36:3	784.7	$C_{18:1}/C_{18:2}$
36:1	788.7	$C_{18:0}/C_{18:1}$
38:6	806.7	$C_{16:0}/C_{22:6}$
38:4	810.7	$C_{18:0}/C_{20:4}$
38:2	812.7	$C_{18:0}/C_{20:2}$
40:7	832.7	$C_{18:1}/C_{22:6}$
40:4	838.7	$C_{18:0}/C_{22:4}$
Ether/Acyl species		*Ether/Acyl*
36:1	772.7	$C_{18:0p}/C_{18:1}$
32:0	718.9	$C_{16:0a}/C_{16:0}$
32:0	718.9	$C_{18:0a}/C_{14:0}$
34:0	744.9	$C_{18:0p}/C_{16:0}$
38:4	794.7	$C_{18:0a}/C_{20:4}$
38:4	794.7	$C_{16:0a}/C_{22:4}$
38:3	796.7	$C_{18:0a}/C_{20:3}$
40:7	816.7	$C_{18:1p}/C_{22:6}$
40:4	822.7	$C_{18:0a}/C_{22:4}$

p = an sn-1 vinyl ether (alkenyl- or plasmalogen) linkage; a = an sn-1 ether (alkyl-) linkage.

follow this prediction early after the impact. In contrast, only molecular species of one class of phospholipids, a $C_{22:6}$-containing CL, underwent oxidation whereas other more abundant phospholipids, particularly PC and PE, remained intact. At a later stage, however, the random character of lipid peroxidation materialized: although CL still remained the preferred peroxidation substrate, other phospholipids, particularly PS, were oxidized as well. This suggests that specific peroxidation mechanisms triggered early after CCI were followed by nonspecific random pathways at later time points.

Although lipid peroxidation has been long associated with brain injury,[10,44] its specific role in mediation of damaging pathways and signaling cascades is not well understood. Recently, signaling functions have been assigned to specific molecular species of oxidized phospholipids.[23,45] We reported that cytochrome *c*–catalyzed CL oxidation products (mostly CL-hydroperoxides [CL-OOH]) accumulate in mitochondria during apoptosis, where they play a critical role in the release of proapoptotic factors into the cytosol.[23] This enzymatic oxidation of CL might explain the specific early accumulation of CL-OOH after injury. Moreover, CL oxidation occurs early in apoptosis in nonneuronal cells preceding cytochrome *c* release, outer mitochondrial membrane permeabilization, caspase activation, and PS externalization.[23] In a separate study, we established that triggering of staurosporine-induced apoptosis in cortical neurons leads to an early and selective CL oxidation, which is not accompanied by oxidation of other more abundant phospholipids.[46] Based on these facts, it is tempting to speculate that selective CL peroxidation early after CCI reflects an initial apoptotic event in brain mitochondria. It is unlikely that CL oxidation originates from a nonspecific inflammatory re-

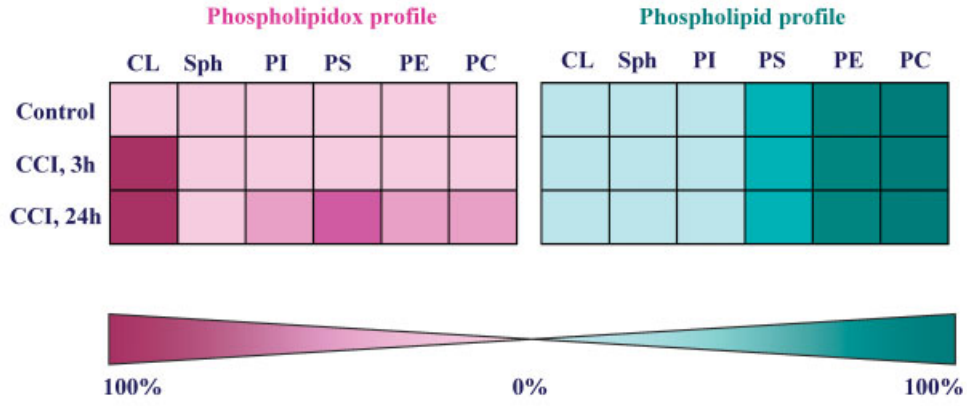

Fig 4. Comparison of the abundance of major phospholipid (PL) classes with their oxidation. Profiles of phospholipids and phospholipid hydroperoxides in control and controlled cortical impact (CCI) ipsilateral cortical P2 fractions. Phospholipid content is expressed as percentage of total phospholipids and shown in green scale. Phospholipid hydroperoxides are presented as percentage of phospholipid (pmol PL-OOH per nmol of phospholipid) and shown in purple scale. One hundred percent corresponds to 110 ± 20pmol of phospholipid hydroperoxide per nanomole of phospholipid. Cardiolipin (CL) was selectively oxidized at 3 hours after CCI, at a time point when other phospholipids were not oxidized. Phosphatidylserine (PS), phosphatidylethanolamine (PE), phosphatidylinositol (PI), and phosphatidylcholine (PC) were oxidized at 24 hours after CCI together with CL. Sph = sphingomyelin.

sponse, which happens much later after CCI.[8] Thus, the early CL oxidation occurs in resident brain cells, likely in mitochondria-rich synaptic and dendritic neuronal projections. Despite accumulation of CL-OOH, we were not able to detect CCI-induced depletion of CL. This is because the amounts of CL-OOH formed represented only a small molar fraction of total CL. This corroborates the role of oxidized CL as an intra-

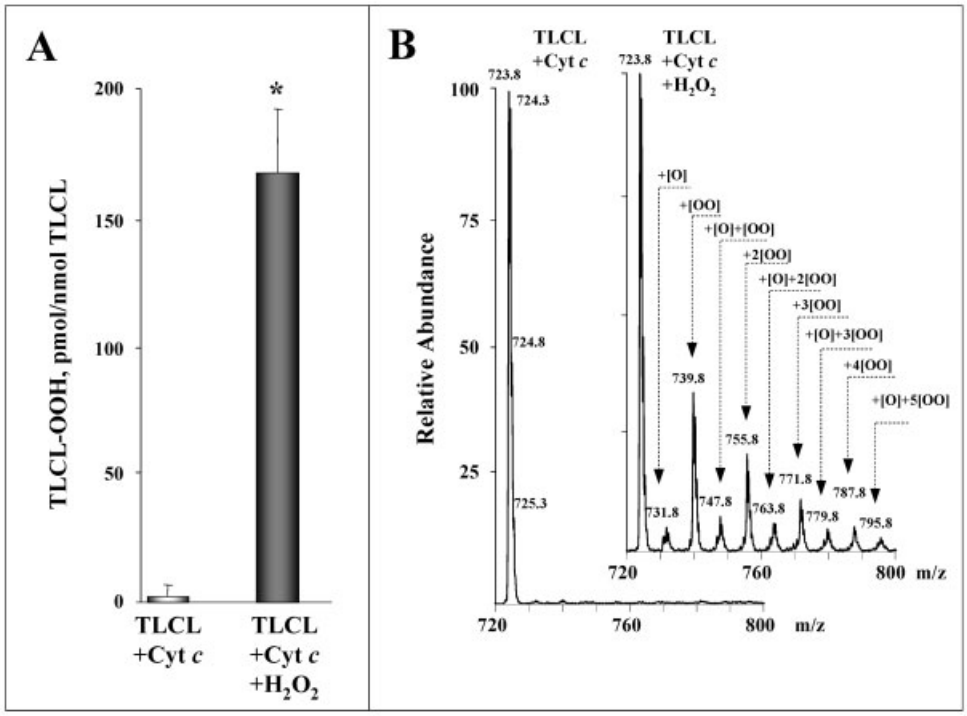

Fig 5. Characterization of cytochrome c (cyt c)–catalyzed peroxidation of tetralinoleyl-cardiolipin (TLCL) in the presence of H_2O_2. Quantitation of the amounts of TLCL-hydroperoxides by fluorescence HPLC-based assay (A). Major oxidation products were identified by ESI mass spectrometry (MS) (B). Molecular species of cardiolipin (CL) containing 1, 2, 3, 4, and 5 hydroperoxy groups were generated in the course of cyt c–catalyzed reaction. In addition, several hydroxy and hydroxy-hydroperoxy derivatives of CL were detected by MS analysis.

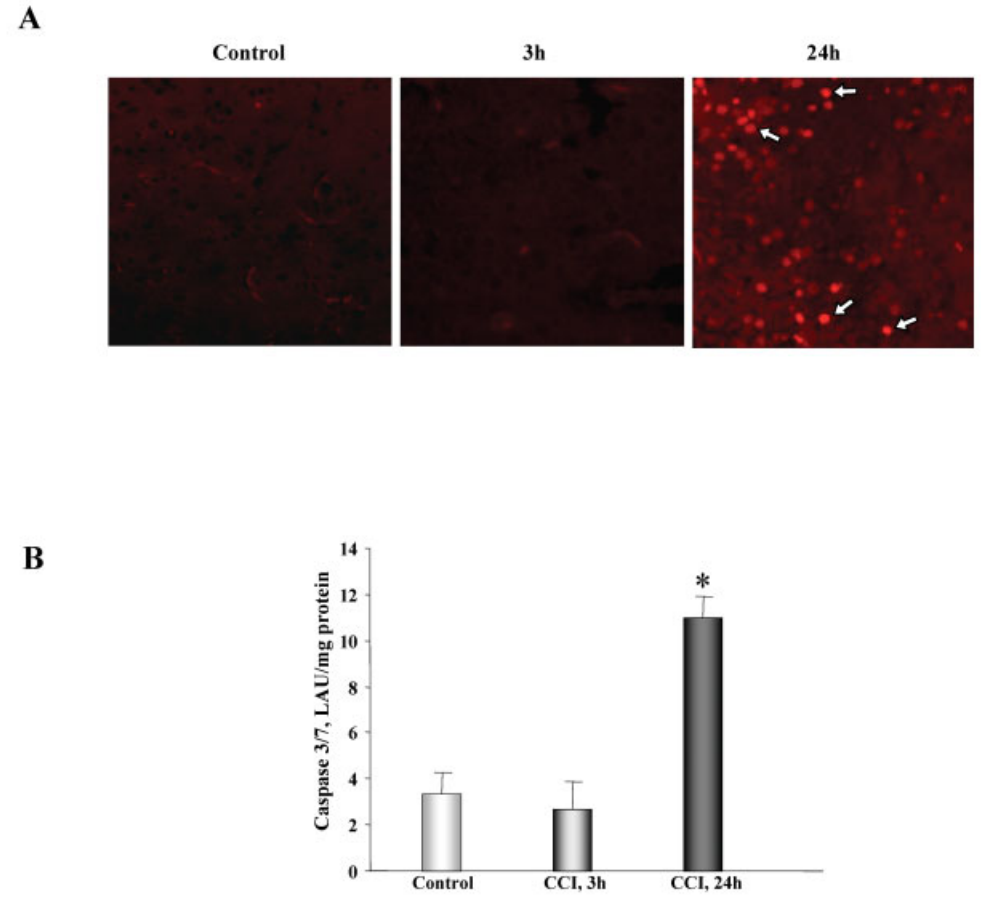

Fig 6. Analysis of cell death in the ipsilateral cortex. (A) Terminal deoxynucleotidyltransferase–mediated dUTP nick end labeling (TUNEL)–positive cells were detected in the ipsilateral pericontusional cortex at 24 hours after controlled cortical impact (CCI) (arrows). *(B) Activity of caspase-3/7, measured in the ipsilateral (left) cortical tissue, was highest at 24-hour injury corroborating the histological data. (n = 5/group; mean ± standard deviation; *p < 0.05 24-hour CCI vs control and 3-hour CCI, analysis of variance).*

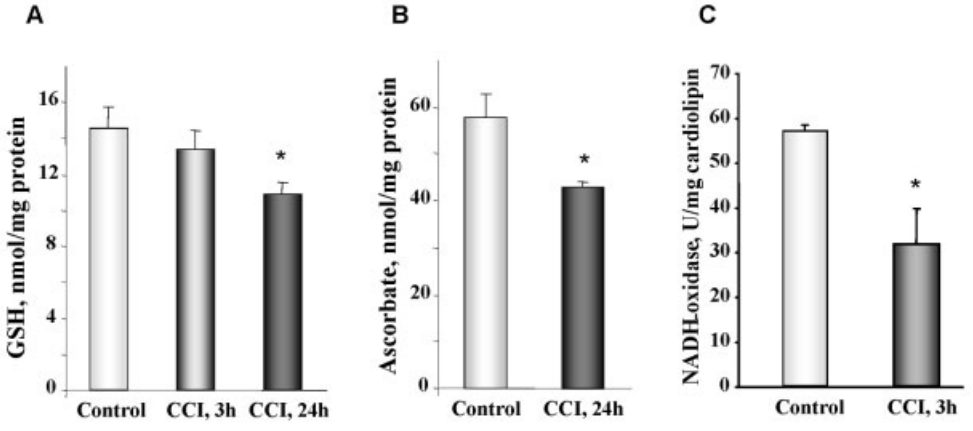

*Fig 7. Assessment of oxidative stress and mitochondrial electron transport activity. Significant decrease in reduced glutathione (GSH) (A) and ascorbate (B) levels in the ipsilateral cortical homogenates were observed at 24 hours after controlled cortical impact (CCI). (n = 5/group; mean ± standard deviation [SD]; *p < 0.05 24-hour CCI vs control for GSH [analysis of variance] and ascorbate [t test]). Rotenone-sensitive NADH:O_2 oxidoreductase activity was decreased in the ipsilateral cortical P2 fractions at 3 hours after CCI versus control. (n = 3/group; mean ± SD; *p < 0.05 3-hour CCI vs control, t test).*

cellular signaling event rather than a random phospholipid oxidation process.

Based on apparent loss of CL, previous work has suggested the involvement of CL oxidation in neuronal proapoptotic responses in vitro.[17,47] Specificity of nonyl acridine orange used in the studies is not sufficient to accurately link changes of its fluorescence characteristics with alterations of CL content and/or peroxidation.[22,48] Therefore, direct estimates of CL oxidation are necessary to prove its participation in neuronal apoptosis. Because CL is a mitochondria-specific phospholipid, our measurements of CL-OOH production rather than CL depletion provide an unequivocal evidence for CL oxidation that takes place in mitochondria. Thus, this work identifies the site (mitochondria), time (3 hours), and molecular species ($C_{22:6}$) of CL peroxidation after TBI. Finally, impairment of mitochondrial electron transport and production of reactive oxygen species are prerequisites for CL oxidation. In line with this we found that mitochondrial electron transport (NADH oxidase) activity was inhibited coincidentally with CL oxidation. This is consistent with our previous demonstration that CL oxidation acts as a switch turning off participation of cytochrome *c* in mitochondrial respiration and turning on its peroxidase function.[49]

Oxidations of Phosphatidylserine and Other Phospholipids: How Specific Are They?

We further established that PS ranked second on the scale of CCI-driven phospholipid oxidation. Again, the molecular species with $C_{22:6}$ was the one that was identifiable in MS as having PS-hydroperoxides (PS-OOH). Although we do not have direct proof for PS oxidation specifically in apoptotic cells, a later accumulation of PS-OOH (24 hours) corresponds with its known role as a signal facilitating PS externalization on the surface of apoptotic cells.[50] This interpretation is also supported by our results demonstrating that caspase-3/7 activation and appearance of TUNEL-positive cells in cortex was coincident with PS oxidation. Because mitochondria do not contain PS, oxidation of this phospholipid could predominantly occur in synaptosomal membranes, further confirming the potential signaling role of PS oxidation in its externalization.[51] At 24 hours after CCI, the most abundant phospholipids, PC and PE, also underwent oxidative modification. It is possible that PC oxidation products act as signaling molecules as well.[45]

TBI causes an increase in the level of free polyunsaturated fatty acid, particularly DHA, in injured brain regions most likely secondary to hydrolysis of phospholipids.[52] Phospholipase A_2 activity increases after TBI.[53] It is possible that oxidation of DHA ($C_{22:6}$)-containing CL and PS stimulates their hydrolysis by phospholipase A_2.[54] However, CL is not a likely source for DHA accumulation because no accumulation of lysoCLs, the products of Phospholipase A_2–catalyzed CL hydrolysis, was detected.

Mitochondrial Electron Transport Activity

Impaired brain mitochondrial function is seen after both experimental and clinical head injury.[1,55–58] Mitochondrial dysfunction begins early and may persist for days after injury. A recent study evaluated the time course of cortical mitochondrial dysfunction in adult mice after CCI and showed concomitant impairment in mitochondrial bioenergetics with accumulation of oxidative stress marker 4-hydroxynonenal as an index of global lipid peroxidation.[59] Our findings expand on these observations to the immature brain and identify one of the major contributors (CL-OOH) to overall lipid peroxidation and mitochondrial dysfunction early after injury.

CL-OOH may represent a new biomarker of oxidative injury possibly associated with an early apoptotic stage of brain damage. Clearance of apoptotic cells in the brain is mediated by oxidation and externalization of PS.[60–62] Because CL oxidation happens before peroxidation of PS, CL-OOH assessments are not likely to be masked by clearance and phagocytosis of apoptotic cells. Further developments of MS analyses can make CL-OOH evaluation in the brain feasible with an imaging protocol.[63] CL oxidation may also represent an important new target for therapeutic intervention. As a selective enzymatic reaction, CL oxidation should not be preventable by lipid antioxidants. Rather, specific disruptors of cytochrome *c*/CL interactions may be promising candidates for this purpose.

We chose to characterize individual molecular species of major phospholipids and their oxidation products after TBI in immature brain rather than adult brain for several reasons. First, trauma is the leading cause of death in children, and severe TBI is an important contributor to this mortality. Studies in pediatric TBI models represent the greatest gap in the literature as delineated by the recently published guidelines for the acute medical management of severe TBI in infants, children, and adolescents.[64] Second, several complex and interrelated pathways of programmed cell death, both caspase-dependent and caspase-independent, can occur after TBI in the developing brain.[65] The relative contribution of each might change with time after the insult and developmental stage of the animal as it has been shown for postnatal day 7 brain versus adult brain after TBI.[66] Third, greater accumulation of phospholipid hydroperoxides is expected in immature versus adult brain after TBI secondary to developmentally low activities of several antioxidant enzymes including GSH peroxidase.[67,68]

Although this study focused on acute brain injury

caused by CCI, it is possible that CL-OOH accumulation occurs in other neurological disorders leading to significant apoptotic cell death. Noteworthy, the appearance of anti-phospholipid antibodies is characteristic of a number of autoimmune diseases predisposing to or associated with brain injury.[69] Recently, it has been demonstrated that anti-CL antibodies recognize oxidized CL more effectively than CL.[70] Direct assessments of CL-OOH and its interactions with anti-phospholipid antibodies may open a new avenue in understanding their role in pathogenesis of central nervous system disorders.

Conclusion

Oxidative lipidomics is a new and exciting tool to study phospholipid oxidative modifications in vivo. Using this technique, we established that CL, specifically its molecular species containing $C_{22:6}$, is selectively oxidized early after TBI, whereas more abundant brain phospholipids remained nonoxidized at this time point. Combined with our previous data, we speculate that accumulation of CL hydroperoxides may be used as a biomarker of apoptosis in vivo that is not masked by effective clearance of apoptotic cells in the brain. Furthermore, the ability to selectively modulate CL oxidation, a critical early event in the mechanism of apoptosis, could lead to targeted therapies and ultimately improve outcome after brain injury.

This work was supported by the American Heart Association (0535365N) (H. Bayir), Laerdal Foundation (H. Bayir), National Institute of Neurological Disorders and Stroke, NINDS (NS30318) (P. Kochanek), National Institute of Allergy & Infectious Diseases, NIAID (U19 AI068021) (V. Kagan), Pennsylvania Department of Health (SAP 4100027294) (V. Kagan), National Institute for Occupational Safety and Health (OH008282) (V. Kagan), Human Frontier Science Program (V. Kagan), and US Army Medical Research and Materiel Command/Telemedicine and Advanced Technology Research Center (DAMD 17-01-2-0038) (P. Kochanek).

References

1. Verweij BH, Muizelaar JP, Vinas FC, et al. Mitochondrial dysfunction after experimental and human brain injury and its possible reversal with a selective N-type calcium channel antagonist (SNX-111). Neurol Res 1997;19:334–339.
2. Uauy R, Hoffman DR, Peirano P, et al. Essential fatty acids in visual and brain development. Lipids 2001;36:885–895.
3. Leitinger N. Oxidized phospholipids as triggers of inflammation in atherosclerosis. Mol Nutr Food Res 2005;49: 1063–1071.
4. Hong S, Lu Y, Yang R, et al. Resolvin D1, protectin D1, and related docosahexaenoic acid-derived products: analysis via electrospray/low energy tandem mass spectrometry based on spectra and fragmentation mechanisms. J Am Soc Mass Spectrom 2007;18:128–144.
5. Jackson SN, Wang HY, Woods AS. In situ structural characterization of glycerophospholipids and sulfatides in brain tissue using MALDI-MS/MS. J Am Soc Mass Spectrom 2007;18: 17–26.
6. Marathe GK, Harrison KA, Murphy RC, et al. Bioactive phospholipid oxidation products. Free Radic Biol Med 2000;28: 1762–1770.
7. Tyurin VA, Tyurina YY, Borisenko GG, et al. Oxidative stress following traumatic brain injury in rats: quantitation of biomarkers and detection of free radical intermediates. J Neurochem 2000;75:2178–2189.
8. Whalen MJ, Carlos TM, Kochanek PM, et al. Neutrophils do not mediate blood-brain barrier permeability early after controlled cortical impact in rats. J Neurotrauma 1999;16: 583–594.
9. Greenwald BD, Burnett DM, Miller MA. Congenital and acquired brain injury. 1. Brain injury: epidemiology and pathophysiology. Arch Phys Med Rehabil 2003;84:S3–S7.
10. Lewen A, Matz P, Chan PH. Free radical pathways in CNS injury. J Neurotrauma 2000;17:871–890.
11. Bayir H, Kagan VE, Tyurina YY, et al. Assessment of antioxidant reserves and oxidative stress in cerebrospinal fluid after severe traumatic brain injury in infants and children. Pediatr Res 2002;51:571–578.
12. Bayir H, Kochanek PM, Liu SX, et al. Increased S-nitrosothiols and S-nitrosoalbumin in cerebrospinal fluid after severe traumatic brain injury in infants and children: indirect association with intracranial pressure. J Cereb Blood Flow Metab 2003;23: 51–61.
13. Meagher EA, FitzGerald GA. Indices of lipid peroxidation in vivo: strengths and limitations. Free Radic Biol Med 2000;28: 1745–1750.
14. Hall ED, Detloff MR, Johnson K, Kupina NC. Peroxynitrite-mediated protein nitration and lipid peroxidation in a mouse model of traumatic brain injury. J Neurotrauma 2004;21:9–20.
15. Bayir H, Marion DW, Puccio AM, et al. Marked gender effect on lipid peroxidation after severe traumatic brain injury in adult patients. J Neurotrauma 2004;21:1–8.
16. Roberts LJ 2nd, Montine TJ, Markesbery WR, et al. Formation of isoprostane-like compounds (neuroprostanes) in vivo from docosahexaenoic acid. J Biol Chem 1998;273:13605–13612.
17. Kirkland RA, Adibhatla RM, Hatcher JF, Franklin JL. Loss of cardiolipin and mitochondria during programmed neuronal death: evidence of a role for lipid peroxidation and autophagy. Neuroscience 2002;115:587–602.
18. Kirkinezos IG, Bacman SR, Hernandez D, et al. Cytochrome *c* association with the inner mitochondrial membrane is impaired in the CNS of G93A-SOD1 mice. J Neurosci 2005;25: 164–172.
19. Fernandez-Gomez FJ, Gomez-Lazaro M, Pastor D, et al. Minocycline fails to protect cerebellar granular cell cultures against malonate-induced cell death. Neurobiol Dis 2005;20:384–391.
20. Garcia Fernandez MI, Ceccarelli D, Muscatello U. Use of the fluorescent dye 10-N-nonyl acridine orange in quantitative and location assays of cardiolipin: a study on different experimental models. Anal Biochem 2004;328:174–180.
21. Jacobson J, Duchen MR, Heales SJ. Intracellular distribution of the fluorescent dye nonyl acridine orange responds to the mitochondrial membrane potential: implications for assays of cardiolipin and mitochondrial mass. J Neurochem 2002;82: 224–233.
22. Gohil VM, Gvozdenovic-Jeremic J, Schlame M, Greenberg ML. Binding of 10-N-nonyl acridine orange to cardiolipin-deficient yeast cells: implications for assay of cardiolipin. Anal Biochem 2005;343:350–352.
23. Kagan VE, Tyurin VA, Jiang J, et al. Cytochrome *c* acts as a cardiolipin oxygenase required for release of proapoptotic factors. Nat Chem Biol 2005;1:223–232.

24. Jenkins LW, Peters GW, Dixon CE, et al. Conventional and functional proteomics using large format two-dimensional gel electrophoresis 24 hours after controlled cortical impact in postnatal day 17 rats. J Neurotrauma 2002;19:715–740.
25. Rice D, Barone S Jr. Critical periods of vulnerability for the developing nervous system: evidence from humans and animal models. Environ Health Perspect 2000;108(suppl 3): 511–533.
26. Weiler MH, Gundersen CB, Jenden DJ. Choline uptake and acetylcholine synthesis in synaptosomes: investigations using two different labeled variants of choline. J Neurochem 1981; 36:1802–1812.
27. Gurd JW, Jones LR, Mahler HR, Moore WJ. Isolation and partial characterization of rat brain synaptic plasma membranes. J Neurochem 1974;22:281–290.
28. Gylys KH, Fein JA, Cole GM. Quantitative characterization of crude synaptosomal fraction (P-2) components by flow cytometry. J Neurosci Res 2000;61:186–192.
29. Folch J, Lees M, Sloane Stanley GH. A simple method for the isolation and purification of total lipides from animal tissues. J Biol Chem 1957;226:497–509.
30. Kagan VE, Ritov VB, Tyurina YY, Tyurin VA. Sensitive and specific fluorescent probing of oxidative stress in different classes of membrane phospholipids in live cells using metabolically integrated cis-parinaric acid. Methods Mol Biol 1998; 108:71–87.
31. Chalvardjian A, Rudnicki E. Determination of lipid phosphorus in the nanomolar range. Anal Biochem 1970;36:225–226.
32. Taguchi R, Hayakawa J, Takeuchi Y, Ishida M. Two-dimensional analysis of phospholipids by capillary liquid chromatography/electrospray ionization mass spectrometry. J Mass Spectrom 2000;35:953–966.
33. Clark RSB, Chen M, Kochanek PM, et al. Detection of single- and double-strand DNA breaks after traumatic brain injury in rats: comparison of in situ labeling techniques using DNA polymerase I, the Klenow fragment of DNA polymerase I, and terminal deoxynucleotidyl transferase. J Neurotrauma 2001;18: 675–689.
34. Langmuir ME, Yang JR, Durand RE. New thiol active fluorophores for intracellular thiols and glutathione measurement. In: Slavik J, ed. Fluorescence microscopy and fluorescent probes. New York: Plenum Press, 1996:229–234.
35. Ritov VB, Menshikova EV, Kelley DE. High-performance liquid chromatography-based methods of enzymatic analysis: electron transport chain activity in mitochondria from human skeletal muscle. Anal Biochem 2004;333:27–38.
36. Gostimskaya IS, Grivennikova VG, Zharova TV, et al. In situ assay of the intramitochondrial enzymes: use of alamethicin for permeabilization of mitochondria. Anal Biochem 2003;313: 46–52.
37. Storrie B, Madden EA. Isolation of subcellular organelles. Methods Enzymol 1990;182:203–225.
38. Ritov VB, Menshikova EV, Kelley DE. Analysis of cardiolipin in human muscle biopsy. J Chromatogr B Analyt Technol Biomed Life Sci 2006;831:63–71.
39. Abdel-Rahman A, Parks JK, Devereaux MW, et al. Developmental changes in newborn lamb brain mitochondrial activity and postasphyxial lipid peroxidation. Proc Soc Exp Biol Med 1995;209:170–177.
40. Sullivan PG, Keller JN, Mattson MP, Scheff SW. Traumatic brain injury alters synaptic homeostasis: implications for impaired mitochondrial and transport function. J Neurotrauma 1998;15:789–798.
41. Urano S, Asai Y, Makabe S, et al. Oxidative injury of synapse and alteration of antioxidative defense systems in rats, and its prevention by vitamin E. Eur J Biochem 1997;245: 64–70.
42. Hsu FF, Turk J. Characterization of cardiolipin from *Escherichia coli* by electrospray ionization with multiple stage quadrupole ion-trap mass spectrometric analysis of [M − 2H + Na]− ions. J Am Soc Mass Spectrum 2006;17: 420–429.
43. Halliwell B. Reactive oxygen species and the central nervous system. J Neurochem 1992;59:1609–1623.
44. Bazan NG, Marcheselli VL, Cole-Edwards K. Brain response to injury and neurodegeneration: endogenous neuroprotective signaling. Ann N Y Acad Sci 2005;1053:137–147.
45. Podrez EA, Poliakov E, Shen Z, et al. Identification of a novel family of oxidized phospholipids that serve as ligands for the macrophage scavenger receptor CD36. J Biol Chem 2002;277: 38503–38516.
46. Bayir H, Tyurin VA, Tyurina YY, et al. A new biomarker of early apoptosis in the brain: cardiolipin oxidation. Toxicol Sci 2006;90:410.
47. Kirkland RA, Franklin JL. Evidence for redox regulation of cytochrome C release during programmed neuronal death: antioxidant effects of protein synthesis and caspase inhibition. J Neurosci 2001;21:1949–1963.
48. Mileykovskaya E, Dowhan W, Birke RL, et al. Cardiolipin binds nonyl acridine orange by aggregating the dye at exposed hydrophobic domains on bilayer surfaces. FEBS Lett 2001;507: 187–190.
49. Basova L, Kurnikov IV, Wang L, et al. Cardiolipin switch in mitochondria: shutting off the reduction of cytochrome *c* and turning on the peroxidase activity. Biochemistry 2007;46: 3423–3434.
50. Jiang J, Serinkan BF, Tyurina YY, et al. Peroxidation and externalization of phosphatidylserine associated with release of cytochrome *c* from mitochondria. Free Radic Biol Med 2003;35: 814–825.
51. Greenberg ME, Sun M, Zhang R, et al. Oxidized phosphatidylserine-CD36 interactions play an essential role in macrophage-dependent phagocytosis of apoptotic cells. J Exp Med 2006;203:2613–2625.
52. Homayoun P, Parkins NE, Soblosky J, et al. Cortical impact injury in rats promotes a rapid and sustained increase in polyunsaturated free fatty acids and diacylglycerols. Neurochem Res 2000;25:269–276.
53. Shohami E, Shapira Y, Yadid G, et al. Brain phospholipase A2 is activated after experimental closed head injury in the rat. J Neurochem 1989;53:1541–1546.
54. Rashba-Step J, Tatoyan A, Duncan R, et al. Phospholipid peroxidation induces cytosolic phospholipase A2 activity: membrane effects versus enzyme phosphorylation. Arch Biochem Biophys 1997;343:44–54.
55. Xiong Y, Gu Q, Peterson PL, et al. Mitochondrial dysfunction and calcium perturbation induced by traumatic brain injury. J Neurotrauma 1997;14:23–34.
56. Sullivan PG, Thompson MB, Scheff SW. Cyclosporin A attenuates acute mitochondrial dysfunction following traumatic brain injury. Exp Neurol 1999;160:226–234.
57. Okonkwo DO, Povlishock JT. An intrathecal bolus of cyclosporin A before injury preserves mitochondrial integrity and attenuates axonal disruption in traumatic brain injury. J Cereb Blood Flow Metab 1999;19:443–451.
58. Robertson CL, Puskar A, Hoffman GE, et al. Physiologic progesterone reduces mitochondrial dysfunction and hippocampal cell loss after traumatic brain injury in female rats. Exp Neurol 2006;197:235–243.
59. Singh IN, Sullivan PG, Deng Y, et al. Time course of posttraumatic mitochondrial oxidative damage and dysfunction in a mouse model of focal traumatic brain injury: implications for neuroprotective therapy. J Cereb Blood Flow Metab 2006;26: 1407–1418.

60. Kagan VE, Gleiss B, Tyurina YY, et al. A role for oxidative stress in apoptosis: oxidation and externalization of phosphatidylserine is required for macrophage clearance of cells undergoing Fas-mediated apoptosis. J Immunol 2002;169:487–499.
61. Adayev T, Estephan R, Meserole S, et al. Externalization of phosphatidylserine may not be an early signal of apoptosis in neuronal cells, but only the phosphatidylserine-displaying apoptotic cells are phagocytosed by microglia. J Neurochem 1998; 71:1854–1864.
62. De Simone R, Ajmone-Cat MA, Minghetti L. Atypical antiinflammatory activation of microglia induced by apoptotic neurons: possible role of phosphatidylserine-phosphatidylserine receptor interaction. Mol Neurobiol 2004;29:197–212.
63. Garrett TJ, Yost RA. Analysis of intact tissue by intermediate-pressure MALDI on a linear ion trap mass spectrometer. Anal Chem 2006;78:2465–2469.
64. Adelson PD, Bratton SL, Carney NA, et al. Guidelines for the acute medical management of severe traumatic brain injury in infants, children, and adolescents. Chapter 1: Introduction. Pediatr Crit Care Med 2003;4:S2–S4.
65. Felderhoff-Mueser U, Sifringer M, Pesditschek S, et al. Pathways leading to apoptotic neurodegeneration following trauma to the developing rat brain. Neurobiol Dis 2002;11:231–245.
66. Bittigau P, Sifringer M, Pohl D, et al. Apoptotic neurodegeneration following trauma is markedly enhanced in the immature brain. Ann Neurol 1999;45:724–735.
67. Fan P, Yamauchi T, Noble LJ, Ferriero DM. Age-dependent differences in glutathione peroxidase activity after traumatic brain injury. J Neurotrauma 2003;20:437–445.
68. Mavelli I, Rigo A, Federico R, et al. Superoxide dismutase, glutathione peroxidase and catalase in developing rat brain. Biochem J 1982;204:535–540.
69. Kanter JL, Narayana S, Ho PP, et al. Lipid microarrays identify key mediators of autoimmune brain inflammation. Nat Med 2006;12:138–143.
70. Horkko S, Olee T, Mo L, et al. Anticardiolipin antibodies from patients with the antiphospholipid antibody syndrome recognize epitopes in both beta(2)-glycoprotein 1 and oxidized low-density lipoprotein. Circulation 2001;103:941–946.